Journal of Alloys and Compounds 856 (2021) 157443

Contents lists available at ScienceDirect

Journal of Alloys and Compounds

journal homepage: http://www.elsevier.com/locate/jalcom

Effect of Mg content in the $La_{3-x}Mg_xNi_9$ battery anode alloys on the structural, hydrogen storage and electrochemical properties

ChuBin Wan [a, b], Weikang Hu [a, c], R.V. Denys [a, d], C.C. Nwakwuo [e], J.K. Solberg [e], V.A. Yartys [a, e, *, 1]

[a] Institute for Energy Technology, P.O. Box 40, Kjeller, NO-2027, Norway
[b] University of Science and Technology Beijing, 100083, China
[c] Zhejiang Normal University, Zhejiang, 321004, China
[d] HYSTORSYS AS, P.O. Box 45, Kjeller, NO-2027, Norway
[e] Norwegian University of Science and Technology, Trondheim, Norway

ARTICLE INFO

Article history:
Received 23 July 2020
Received in revised form
27 September 2020
Accepted 1 October 2020
Available online 3 October 2020

Keywords:
Hydrogen storage materials
Metal hydride batteries
La–Mg–Ni alloys
Anode electrodes
Crystal structure

ABSTRACT

The present work is focused on the studies of structure, hydrogen storage and electrochemical properties of the $La_{3-x}Mg_xNi_9$ (x = 1.0, 1.1 and 1.2) alloys as active materials of negative electrodes in the Nickel-Metal Hydride (Ni/MH) batteries. A change of Mg content affects properties of the studied alloys such as the phase homogeneity, hydrogen storage and electrochemical capacities, cycle stability, and high-rate discharge performance. X-ray diffraction study shows that Mg substitution for La and annealing of the $La_{3-x}Mg_xNi_9$ alloys promotes the formation of more homogeneous materials, with a predominant formation of the target AB_3 $PuNi_3$ structure type intermetallics. The electrodes prepared from the annealed alloys show the maximum discharge capacities of ~400 mAh g^{-1} at discharge current density of ~60 mA/g. The high rate discharge-abilities (HRD) at the discharge current density of 350 mA g^{-1} keep high values of the remaining reversible discharge capacities, ~86, 85 and 80%, for the La_2MgNi_9, $La_{1.9}Mg_{1.1}Ni_9$ and $La_{1.8}Mg_{1.2}Ni_9$ alloy electrodes, respectively. After 200 cycles with 100% depth of discharge (DOD), the $La_{1.9}Mg_{1.1}Ni_9$ alloy electrode exhibits a very good cycling stability with its discharge capacity remaining at a level of ~64% of its initial capacity.

© 2020 The Authors. Published by Elsevier B.V. This is an open access article under the CC BY license (http://creativecommons.org/licenses/by/4.0/).

1. Introduction

Hydrogen energy has a great potential in generating clean power in efficient way and is currently utilized in stationary, portable and transport applications [1,2]. Among various technologies used to store hydrogen, metal hydrides, which were studied and developed during the last 50 years, are recognized as a volume-efficient hydrogen storage technology which is highly suitable for energy storage and conversion systems, particularly when utilized in Ni-MH battery applications [2,3].

Among various types of hydrides, Mg and Mg-based compounds have been intensively studied due to the favorable low cost of Mg metal as a raw material and high gravimetric (7.6 wt % H in MgH_2) and volumetric (110 g_H/L in MgH_2) hydrogen storage densities [4,5].

Within the Mg-based alloys, RE-Mg-Ni intermetallics (RE = Rare Earth Metals), including $(RE,Mg)Ni_3$ [6–8], $(RE,Mg)_2Ni_7$ [9,10] and $(RE,Mg)_5Ni_{19}$ [11,12] compounds, attract significant interest as active materials for the anodes of the Ni/MH batteries. All these intermetallics belong to the layered hybrid structures which are formed by stacking on the top of each other of the $RENi_5$ layers with $CaCu_5$ type of structure and $(RE,Mg)Ni_2$ layers with Laves type structure. However, the ratio between $RENi_5$ and $(RE,Mg)Ni_2$ layers changes as related to the type of intermetallic; 3 $(RE,Mg)Ni_3$ = $RENi_5$ + 2 $(RE,Mg)Ni_2$; $(RE,Mg)_2Ni_7$ = $RENi_5$ + $(RE,Mg)Ni_2$; $(RE,Mg)_5Ni_{19}$ = 3 $RENi_5$ + 2 $(RE,Mg)Ni_2$. Formation of the layered Mg-containing RE-Mg-Ni intermetallics is associated with the formation of the extensive solid solutions of Mg by substituting RE in the $RENi_2$ layers. At the same time, increase of Mg content improves the electrochemical properties of these alloys used as battery anodes in the Ni-MH batteries, including increase in their electrochemical discharge capacity, easy activation and improved high-rate

* Corresponding author. Institute for Energy Technology, P.O. Box 40, Kjeller, NO-2027, Norway.
E-mail address: volodymyr.yartys@ife.no (V.A. Yartys).
[1] This paper is #100 among the publications by Prof. V.A. Yartys in Journal of Alloys and Compounds.

https://doi.org/10.1016/j.jallcom.2020.157443
0925-8388/© 2020 The Authors. Published by Elsevier B.V. This is an open access article under the CC BY license (http://creativecommons.org/licenses/by/4.0/).

dischargeability.

Recently, a significant research effort has been devoted to the studies of the RE-Mg-Ni alloys for Ni-MH battery applications. 1:3, 2:7 and 5:19 intermetallics all show suitable performance as battery anodes, particularly because their electrochemical discharge capacities of 392 for La_2MgNi_9, 386 for La_3MgNi_{14} and 367 for La_4MgNi_{19} are superior as compared to 320 mAh/g characteristic for the commercial AB_5 type Co-containing alloys [13].

In our earlier studies, ternary RE-Mg-Ni and RE-Mg-(Ni,Mn) intermetallics crystallizing with the $PuNi_3$ trigonal type of structure were systematically studied as hydrogen storage materials and anode electrode materials for Ni/MH batteries. These studies showed that Mg atoms substitute RE atoms in RE-Mg-Ni compounds entering the AB_2 [$RE(Ni,Mn)_2$] slabs only, while Mn atoms mostly replace Ni atoms in the AB_5 [$RE(Ni,Mn)_5$] slabs, with small amount of Mn being located in the Kagome nets joining the AB_2 and AB_5 slabs [14]. Because of the stabilization of the metal sublattice by Mg, the studied alloys do not show amorphization and disproportionation during the prolonged cycling of hydrogen absorption and desorption [15] thus allowing to achieve long cycle and calendar life of the alloys used in H storage and electrochemical applications.

Mg content has a strong effect of the properties of $RE_{3-x}Mg_xNi_9$ intermetallics as H storage materials. Both AB_2 and AB_5 slabs undergo a significant volume contraction; a contraction level linearly increases following the increase of the Mg/La ratio [16]. Studies of the hydrogenation behaviors showed that for the AB_3-type $La_{3-x}Mg_xNi_9$ [16] alloys a substitution of La by Mg decreased the stability of the hydrides, with equilibrium hydrogen desorption pressures changing at room temperature from 0.011 bar (for $La_{2.3}Mg_{0.7}Ni_9$) to 18 bar (for $La_{1.0}Mg_{2.0}Ni_9$) H_2. The highest reversible hydrogen storage capacity, 1.58 wt% H, has been reached for a La_2MgNi_9 alloy, with half of La in AB_2 slabs being substituted by Mg.

The substitutions of La by Nd, Pr and Mg were studied for the $RE_{3-x}Mg_xNi_9$ (RE = La, Nd and Pr; x = 1.0–1.2) intermetallics and showed that they are efficient anodes for the rechargeable Ni-metal hydride batteries [17]. A partial substitution of Mg for RE and of La for Nd and Pr improved the discharge capacity to reach 400 mAh/g (@ 60 mA/g) and with almost 50% capacity remaining after 300 cycles (with 100% DOD) [6,8,18]. In the $(La, Nd)_2MgNi_9$ alloys, the presence of Nd improved the properties of the anode electrodes, including appearance of the broader and flatter plateaus, higher H exchange rates, better cycling stability and better performance at high discharge current rates [6,8,19].

When changing the type of the layered structure from 1:3 to 5:19 intermetallic, the $(La,Mg)_5Ni_{19}$ phase is formed and its formation enhances the cycling stability and high rate dischargeability of the La–Mg–Ni-based alloys, which is ascribed to its higher structural stability and higher hydrogen desorption plateau pressure [9], however together with a decrease in the discharge capacity.

A partial substitution of La with Sm in the $La_{0.63}Sm_{0.2}Mg_{0.17}Ni_{3.1}Co_{0.3}Al_{0.1}$ alloy resulted in the increased abundance of the 2:7 Ce_2Ni_7-type phase, which leads to the improved cycle and high rate discharge ability. The optimized alloy exhibited good overall electrochemical discharge capacity (393.3 mAh g^{-1}) and cycling retention (87.2% after 100 cycles) [20].

On the other hand, effect of substitution of Ni by Co has been studied in a multiphase AB_3 type $La_2MgNi_7Co_2$ alloy. This alloy showed an increased hydrogen storage capacity of 1.90 wt% H (@ 10 bar H_2) [21].

Further to the effect of chemical composition by using substitutions, in our earlier studies, we showed that phase-structural composition of RE-Mg-Ni samples has a strong influence on their H storage and electrochemical behaviors. In particular, properly annealed alloys have superior behaviors as compared to the as cast alloys [22]. When annealing temperature equals to 950 °C, this leads to the highest abundance of La_2MgNi_9 and La_3MgNi_{14} phases in La_2MgNi_9 alloys and improves the electrochemical performances, with a full discharge capacity of ~400 mAh/g and cycling stability retaining 50% after 300 cycles in half-cell tests [22]. When applying rapid solidification, it is possible to control the Mg content and to synthesize an optimized from the point of view of electrochemical performance La_2MgNi_9 alloy [23].

By controlling the precursor ratio ($LaMgNi_4$/$La_{0.60}Gd_{0.15}Mg_{0.25}Ni_{3.60}$), the single-phase $PuNi_3$-, Ce_2Ni_7-, Pr_5Co_{19}-type La-Gd-Mg-Ni based alloys can be prepared by a powder sintering method at 1203 K. The electrochemical discharge capacity of the Pr_5Co_{19}-type electrode could reach 200 mAh g^{-1} at a very high current density of 1800 mA g^{-1} [24]. Hence, the RE-Mg-Ni alloys can be considered as having a great potential alloy materials for hydrogen storage and metal hydride batteries.

Optimal conditions of homogenization of the alloys were found in our earlier work [7], where La–Mg–Ni alloys were studied *in situ* during their heating while performing neutron diffraction study in a neutron beam. *In situ* study allowed to determine the mechanism of the phase-structural transformations during the annealing at high temperatures [7,8,25]. Several peritectic reactions take place in sequence in the La_2MgNi_9 and $La_{1.5}Nd_{0.5}MgNi_9$ alloys in a temperature range from 300 K to 1273 K [7,8].

Based on *the in situ* temperature-dependent neutron diffraction study, the increase of Mg amount leads to a continuous shrinking of unit cells for all studied alloys and to the phase-structural transformations involving AB_5, A_2B_4, AB_3, A_2B_7 and A_5B_{19}-type intermetallics [7]. AB_3 $PuNi_3$-type structures appear to be the major constituent of a multiphase alloys. Interestingly, only one modification from two known, rhombohedral 3R structure A_2B_7, was experimentally observed during the annealing while a polymorphic transformation from a low temperature to the high temperature modifications was observed in case of the A_5B_{19} compounds [7,8].

Furthermore, use of neutron diffraction allowed to determine the crystal structures of the RE-Mg-Ni hydrides based on the $PuNi_3$ type of structure of the initial intermetallic alloy. The saturated by hydrogen $La_2MgNi_9D_{13.1}$ hydride has been found to form via an isotropic expansion of the initial unit cell of the intermetallic alloy and crystallizes with a trigonal (space group R-3m) unit cell [26]. D (H) atoms are equally distributed between the $REMgNi_4$ and $RENi_5$ layers; while local hydrogen ordering takes place in the hydrides, with hydrogen sublattice being built from the MgH_6 octahedra and NiH_4 tetrahedra [17,26].

Hydrogen storage and electrochemical properties of La_2MgNi_9 alloys were most extensively studied for La_2MgNi_9 alloy which exhibits superior reversible capacity and a suitable for use in the metal hydride batteries equilibrium pressure of H_2 absorption-desorption (at 293 K, abs. P = 0.095 bar/des. P = 0.045 bar H_2) [16]. Therefore, it is important to make a more comprehensive investigation of the impact of Mg substitution for La on the properties of the $La_{3-x}MgxNi_9$-based alloy.

In the present study, the crystal structure, hydrogen absorption-desorption, and electrochemical properties are systematically studied as related to the variable Mg content by changing the La/Mg ratio. The focus was on a detailed study of the $La_{3-x}Mg_xNi_9$ intermetallics containing Mg at amounts x = 1.0, 1.1 and 1.2. The objective is in finding an interrelation between the Mg content and the electrochemical performance of the $La_{3-x}Mg_xNi_9$ alloys as anodes of the Nickel/Metal Hydride batteries.

2. Experimental

2.1. Preparation of the $La_{3-x}Mg_xNi_9$ alloys and their structural characterization

The precursor La–Mg–Ni alloys were prepared by intermediate frequency induction melting from the starting elementary metals with a purity of not less than 99.5% under a protective gas atmosphere. In order to achieve a control over the Mg content and to reduce vaporization of magnesium during the smelting processes, Helium gas was used as a protective gas while the amount of magnesium metal used to prepare the alloy contained appr. 3% excess of Mg as compared to the stoichiometric composition. After the induction melting, the melt was poured into a water-cooled copper mould. As-cast alloy ingots, about 3 kg per batch, were obtained.

The alloy ingots were crushed into pieces of about 5–10 mm in diameter. Subsequently the pieces were sealed in argon filled stainless steel cylindrical tubes and were annealed at 950 °C for 6 h before quenching the tubes into an iced water.

The quenched alloys were then further ground into the powders with particles size of 40–60 μm which were used in the electrochemical measurements and for the phase-structural analysis. X-ray diffraction (XRD) with Cu $K\alpha_1$ radiation was used to identify the phase structure and composition of the alloys as well as their crystalline state. The XRD data were collected using a Bruker D8 DISCOVER diffractometer with a Ge-monochromator and a LYNX-Eye detector. The morphology and phase composition of the alloys were analyzed using a Zeiss Supra 55 VP scanning electron microscope (SEM) with a field emission gun (FEG) and equipped with a Bruker EDX detector. The samples were embedded into polyfast resin with carbon filler and prepared by grinding in successive steps, and polishing. In order to enhance phase contrast images were obtained in the backscattered electron (BSE) mode. For accurate chemical analysis of the samples, ZAF corrections were also applied to the EDX spectroscopy data.

2.2. PCT studies and hydrogen storage characterization

Hydrogen absorption-desorption properties of the alloys were characterized using a Sieverts type system. The samples were activated in vacuum at 523 K for 30 min, cooled to 293 K and then charged with a high purity hydrogen gas (99.999%). Pressure-Composition-Temperature (PCT) dependences of hydrogen absorption and desorption were measured on the activated samples at 293 K and H_2 pressures from 0.005 to 10 bar H_2.

2.3. Preparation of MH electrodes and electrochemical measurements

Electrochemical properties were tested in a three-electrode system with a 9 N KOH solution electrolyte at room temperature. The system consisted of a metal hydride (MH) working electrode, a sintered $NiOOH/Ni(OH)_2$ counter electrode with a larger than the MH electrode capacity and a Hg/HgO (9 N KOH) reference electrode.

The MH electrodes were first activated at a 0.1 C rate for three charge-discharge cycles. Then, the rate capability and cycling stability were evaluated galvanostatically. Each electrode was fully charged at a 0.1 C rate and then the rate capability and cycling stability were evaluated, and the cut-off potential of the discharge was set at −0.74 V vs the Hg/HgO electrode (1 C = 300 mAh/g).

The electrodes were prepared as pasted electrodes and alternatively also pressed as pellets. Pasted MH electrodes were prepared in the following steps: (a) mixing of the alloy powder (40–60 μm particles) with a fine graphite powder in a weight ratio of 10:1 and then adding 3% PTFE solution as a binder to make a paste; (b) the mixture was then pasted on a Ni foam substrate with a size of 30 × 30 × 1.5 mm with a nickel strip welded on to the foam in advance; (c) after the drying, it was cold pressed with an extra Ni foam forming a sandwich structure.

Pellet MH electrodes were prepared by mixing MH alloy powder having a particle size of 40–60 μm with carbonyl Ni powder with a surface area of ~0.7 m^2/g. The weight ratio of MH alloy to carbonyl nickel powder was chosen as 1:4. The pellet electrode was made by cold-pressing of the powder mixture into a pellet under a pressure of 10 MPa with a diameter of 10 mm and then sandwiched between two Ni foams which were welded to a nickel strip.

3. Results and discussion

3.1. Phase-structural analysis for the alloys

3.1.1. As cast $La_{3-x}Mg_xNi_9$ alloys

As listed in Table 1, XRD study of the as cast alloys showed the presence of intermetallics crystallizing with 6 different types of structures including $PuNi_3$, Gd_2Co_7, Ce_5Co_{19}, Pr_5Co_{19}, $MgCu_4Sn$ and $CaCu_5$ types. As can be seen from the data of Rietveld profile refinements, $PuNi_3$-type $La_{3-x}Mg_xNi_9$ intermetallics were a majority phase in each studied case (43.9–58.1 wt%). With the increase of Mg content, the abundance of target $PuNi_3$-type compound increases in the as-cast $La_{3-x}Mg_xNi_9$ alloys. However, a significant amount of $LaNi_5$ was present in each as cast alloy, 19.3–28.3 wt%. Furthermore, $MgCu_4Sn$-type AB_2 compounds were observed in all studied alloys, at the content of 6.7–13.6 wt%. The Rietveld refinements of XRD pattern of the as-cast $La_{3-x}Mg_xNi_9$ (x = 1.1 and 1.2) alloys were performed using GSAS software [27] and the results are shown in Fig. S1 in Supplementary Materials.

3.1.2. Annealed at 1223 K $La_{3-x}Mg_xNi_9$ alloys

The data of the refinements of the XRD patterns (measured at 300 K) of the annealed at 1223 K samples is shown in Fig. 1. From analysis of the data given in Table 2, it can be concluded that after the annealing, the content of $PuNi_3$ type structure vastly increased for each studied alloy, with its amount exceeding 88 wt% for $La_{1.8}Mg_{1.2}Ni_9$ alloy. $PuNi_3$ and Gd_2Co_7-type intermetallics together formed an overwhelming majority, > 90 wt% in each studied case. At the same time, amount of Mg-free $LaNi_5$ dramatically decreased to below 5 wt% for each alloy.

$La_{1.8}Mg_{1.2}Ni_9$ alloy exhibits presence of a nearly-homogeneous single $(La,Mg)Ni_3$ phase (~89 wt%); furthermore, $(La,Mg)_2Ni_7$-3R and $LaNi_5$ are the minor phases. We also observe that no $MgCu_4Sn$-type $(La,Mg)_2Ni_4$ intermetallic is present in the studied annealed alloys. Thus, annealing treatment is helpful to deplete $LaNi_5$ and $(La,Mg)_2Ni_4$ phases. We believe that a homogeneous single phase $(La,Mg)Ni_3$ alloy can be obtained by optimizing the Mg content and the conditions of the annealing treatment.

Moreover, among the studied annealed alloys, with the increase of Mg content, the unit cell parameters *a*, *c* and volumes of the $(La,Mg)Ni_3$ unit cells show a continuous decrease, as shown in Fig. 2. Reference lattice parameters of $PuNi_3$-type $(La,Mg)Ni_3$ phases are taken from our earlier works [16,17]. The shrinking of the volumes of the unit cells was caused by the substitution of La by Mg. This is as expected, because of an obvious difference between the atomic radii of La (1.87 Å) and Mg (1.60 Å); thus, the unit cell dimensions (*a* and *c*) for $La_{1.9}Mg_{1.1}Ni_9$ and $La_{1.8}Mg_{1.2}Ni_9$ phase are slightly lower, by 0.1–0.3%, as compared to La_2MgNi_9 phase.

In the La–Mg–Ni superlattice structures built from the stacking of the $CaCu_5$ (AB_5) and Laves type layers (A_2B_4), Mg atoms enter only the [A_2B_4] slabs, with no La substitution by Mg taking place within the $CaCu_5$ type layers. This means that Mg exclusively

Table 1
Phase-structural composition of as-cast $La_{3-x}Mg_xNi_9$ alloys from XRD analysis.

Sample	Phase	Type of structure	Sp.gr.	Unit cell parameters, Å		Abundance, wt.%
				a	c	
La_2MgNi_9 (as cast) [22]	La_2MgNi_9	$PuNi_3$	$R\bar{3}m$	5.0320(1)	24.2885(9)	43.9(3)
	La_3MgNi_{14} -3R	Gd_2Co_7	$R\bar{3}m$	5.0298(6)	36.234(5)	16.4(5)
	La_4MgNi_{19} -3R	Ce_5Co_{19}	$R\bar{3}m$	5.0272(7)	48.194(7)	7.4(4)
	La_4MgNi_{19}—2H	Pr_5Co_{19}	$P6_3/mmc$	5.026(2)	32.10(1)	3.6(3)
	$LaMgNi_4$	$MgCu_4Sn$	$F\bar{4}3m$	7.1671(2)	–	9.4(1)
	$LaNi_5$	$CaCu_5$	$P6/mmm$	5.0274(2)	3.9877(1)	19.3(2)
$La_{1.9}Mg_{1.1}Ni_8$ (as cast)	$La_{1.9}Mg_{1.1}Ni_9$	$PuNi_3$	$R\bar{3}m$	5.0295(3)	24.266(3)	44.2(4)
	$La_{2.9}Mg_{1.1}Ni_{14}$ -3R	Gd_2Co_7	$R\bar{3}m$	5.0255(4)	36.192(3)	22.9(7)
	$La_{0.9}Mg_{1.1}Ni_4$	$MgCu_4Sn$	$F\bar{4}3m$	7.1663(4)	–	6.7(2)
	$LaNi_5$	$CaCu_5$	$P6/mmm$	5.0271(2)	3.9874(2)	26.2(5)
$La_{1.8}Mg_{1.2}Ni_9$ (as cast)	$La_{1.8}Mg_{1.2}Ni_9$	$PuNi_3$	$R\bar{3}m$	5.0188(2)	24.176(2)	58.1(3)
	$La_{0.8}Mg_{1.2}Ni_4$	$MgCu_4Sn$	$F\bar{4}3m$	7.1433(4)	–	13.6(5)
	$LaNi_5$	$CaCu_5$	$P6/mmm$	5.0288(3)	3.9884(2)	28.3(5)

occupies the Laves type layer, substituting half of La atoms in $PuNi_3$-type La_2MgNi_9 phase at maximum. This suggests that when Mg content increases from 1.0 to 1.2, the La substitution by Mg increases continuously in the $[A_2B_4]$ slabs. Hence, the unit cell volume of the $PuNi_3$-type phase continues to decrease from 531.86 to 529.29 $Å^3$ (~0.5%). The relatively high temperature of the annealing treatment, 1223 K, as compared to the melting temperature of magnesium metal, 923 K, ensures a quick enough kinetics to allow homogenization of the $(La,Mg)Ni_3$ phase with evenly distributed magnesium in the sample. Absence of the $MgCu_4Sn$-type phase indicates that this phase is unstable at such high annealing temperature of 1223 K.

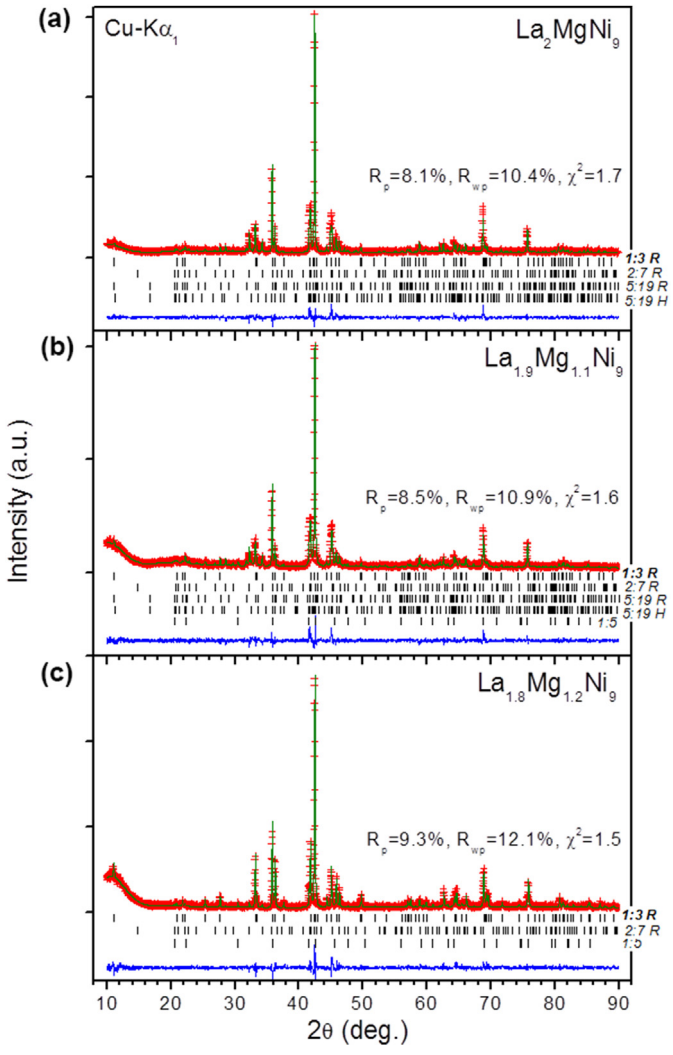

Fig. 1. X-ray diffraction patterns (Cu-$K_{\alpha 1}$ radiation) of the annealed La_2MgNi_9, $La_{1.9}Mg_{1.1}Ni_9$ and $La_{1.8}Mg_{1.2}Ni_9$ alloys measured at 300 K. Vertical bars show positions of the Bragg peaks for the phase constituents. The 1:3 R, 2:7 R, 5:19 R, 5:19 H, and 1:5 abbreviations represent the $(La,Mg)Ni_3$, $(La,Mg)_2Ni_7$-3R, $(La,Mg)_5Ni_{19}$-3R, $(La,Mg)_5Ni_{19}$—2H and $LaNi_5$ phases.

The La—Mg—Ni intermetallics, such as $(La,Mg)Ni_3$, $(La,Mg)_2Ni_7$ and $(La,Mg)_5Ni_{19}$, stack along the *c*-axis with different ratios of $[(La,Mg)_2Ni_4]$ and $[LaNi_5]$ subunits. As described above, when Mg atoms are introduced into the super-stacked structures, La replacement by Mg proceeds only within the Laves-type subunits. This indicates that the solid solubility of Mg decreases when the ratio between $LaNi_5$ and $(La,Mg)_2Ni_4$ subunits increases in $(La,Mg)_2Ni_7$ and $(La,Mg)_5Ni_{19}$ phases. When Mg content reaches a significantly high amount, it becomes favorable to form a $(La,Mg)Ni_3$ phase with a relatively high solid solubility of Mg, as shown in the present study (x = 1.2).

Furthermore, we note that the abundance of the $PuNi_3$-type phase can reach 100 wt% after the annealing performed at 1073 and 873 K for 16 h, as in the annealed $La_{3-x}Mg_xNi_9$ (x = 0—2) alloys, when x equals 1.5, as in our earlier work [16]. This suggests that controlling the Mg content and choosing appropriate annealing conditions is an effective way to prepare single pase $PuNi_3$-type alloys.

In $Nd_{3-x}Mg_xNi_9$ (x = 0.3—1.5) alloys [28], with x equal to 1.2, when La is replaced by Nd, the single phase $PuNi_3$-type alloy was obtained after the annealed at 1183 K for 4 days. Furthermore, in $Pr_{3-x}Mg_xNi_9$ (x = 0.45—1.2) alloys [29], the homogeneous Pr_2MgNi_9 (x = 1.0) alloy contained 100 wt% $PuNi_3$-type phase after annealing at 1173 K for 4.8 days. These differences in the behavior may be associated with the different solid solubility of Mg in the $(La,Mg)_2Ni_4$, $(Nd,Mg)_2Ni_4$ and $(Pr,Mg)_2Ni_4$ slabs.

It is interesting that *a* value of $LaNi_5$ phase quite significantly decreases for x = 1.2. This can be attributed to the possible variations of stoichiometry of $LaNi_{5\pm x}$, (increase of Ni content to form an overstoichiometric $LaNi_{5+x}$); this suggestion requires further analysis using SEM/EDX data (see Fig. S3 in the Supplementary Material file).

Further to the XRD data, we have also collected and analyzed the data from the *in situ* NPD study of the annealing process for the alloys performed from ambient temperature up to 1223 K. The results of the Rietveld refinements are listed in Table S1. It becomes

Table 2
Phase-structural composition of the annealed $La_{3-x}Mg_xNi_9$ alloys.(annealing was performed at 1223 K for 6 h in Ar).

Sample	Phase	Type of structure	Sp.gr.	Unit cell parameters, Å		Abundance, wt.%
				a	c	
La_2MgNi_9 (annealed) [22]	La_2MgNi_9	$PuNi_3$	$R\bar{3}m$	5.0304(1)	24.2625(8)	51.1(3)
	La_3MgNi_{14} -3R	Gd_2Co_7	$R\bar{3}m$	5.0336(1)	36.279(1)	39.9(4)
	La_4MgNi_{19} -3R	Ce_5Co_{19}	$R\bar{3}m$	5.031(−)	48.30(−)	5.9(4)
	La_4MgNi_{19}−2H	Pr_5Co_{19}	$P6_3/mmc$	5.033(−)	32.14(−)	3.1(3)
$La_{1.9}Mg_{1.1}Ni_8$ (annealed)	$La_{1.90(2)}Mg_{1.10(2)}Ni_9$	$PuNi_3$	$R\bar{3}m$	5.0279(3)	24.232(2)	48.8(4)
	$La_{2.9}Mg_{1.1}Ni_{14}$ -3R	Gd_2Co_7	$R\bar{3}m$	5.0297(4)	36.246(3)	33.9(5)
	La_4MgNi_{19} -3R	Ce_5Co_{19}	$R\bar{3}m$	5.030(1)	48.24(1)	10.3(6)
	La_4MgNi_{19}−2H	Pr_5Co_{19}	$P6_3/mmc$	5.032(−)	32.15(−)	4.7(6)
	$LaNi_5$	$CaCu_5$	$P6/mmm$	5.033(2)	3.993(2)	2.3(2)
$La_{1.8}Mg_{1.2}Ni_9$ (annealed)	$La_{1.80(1)}Mg_{1.20(1)}Ni_9$	$PuNi_3$	$R\bar{3}m$	5.0190(2)	24.187(1)	88.6(8)
	$La_{2.8}Mg_{1.2}Ni_{14}$ -3R	Gd_2Co_7	$R\bar{3}m$	5.0291(7)	36.177(7)	7.3(4)
	$LaNi_5$	$CaCu_5$	$P6/mmm$	5.0257(5)	3.994(1)	4.1(3)

evident that almost all the $(La,Mg)_5Ni_{19}$ and $(La,Mg)_2Ni_7$ phases transformed into $(La,Mg)Ni_3$ phase in $La_{1.8}Mg_{1.2}Ni_9$ alloy during the annealing followed by the quenching and it indicates that the transformation $(La,Mg)_5Ni_{19}$ 3R/2H + $(La{\cdot}Mg)_2Ni_4$ → $(La,Mg)_2Ni_7$ → $(La,Mg)Ni_3$ proceeds in all studied alloys. However, for the $La_{1.8}Mg_{1.2}Ni_9$ alloy, the phase transformations indicate that the $(La,Mg)Ni_3$ phase is the last end-product formed before the quenching.

For R_2Ni_7 alloys an intermetallic compound with Ce_2Ni_7 type (2H) structure has been identified as a low temperature modification while intermetallic crystallizing with Gd_2Co_7 type (3R) modification is formed as the high temperature phase. In our earlier study [15], a single phase Ce_2Ni_7-type $La_{1.5}Mg_{0.5}Ni_7$ alloy has been obtained by powder sintering and annealing for 4 days at 750 °C, which agrees with the suggestion that the Ce_2Ni_7 type (2H) is the low temperature modification.

In the present work, the $La_{3-x}Mg_xNi_9$ alloys were prepared by induction melting followed by their annealing at 950 °C. At such high temperature equilibrium conditions a formation of A_2B_7-3R (Gd_2Co_7-type) as a secondary phase (further to the main rhombohedral $PuNi_3$ type $(La,Mg)_3Ni_9$ intermetallic) was observed in both as cast and annealed samples, in line with a suggestion that 3R type intermetallic is a high temperature modification. Absence of the 2H type intermetallic in these alloys is because the annealing temperature is outside of the stability range of the low temperature A_2B_7−2H modification.

A related reference publication revealing results of the study of the $La_{1.5}Mg_{0.5}Ni_7$ alloy by Zhang et al. [30] reported that the alloy cast from the melt contained only a 3R Gd_2Co_7-type high temperature modification of the A_2B_7 phase, while the samples further annealed for 24 h at 800–900 °C consisted of both Gd_2Co_7 and Ce_2Ni_7 types, indicating that on cooling down a transformation from 3R to 2H modifications occurred in this mentioned temperature range. Thus, it is obvious that a careful control over the preparation conditions is required to achieve a formation of either A_2B_7-3R or A_2B_7−2H phases (or their mixture) as related to the temperature and time of the annealing process.

3.1.3. SEM characterization

From the SEM images, the as-cast and annealed La_2MgNi_9, $La_{1.9}Mg_{1.1}Ni_9$ and $La_{1.8}Mg_{1.2}Ni_9$ alloys possess a segregated multiphase structure with coarse grains as is shown in Figs. 3 and 4.

To identify the phases present in the samples, EDX spectroscopy study was performed and three distinct phases are clearly visible in the microstructure. The as-cast alloys mainly consist of $(La,Mg)Ni_3$, $LaNi_5$, and $(La,Mg)_2Ni_4$ phases. The $(La,Mg)_2Ni_7$ phase was also observed in the as-cast La_2MgNi_9 alloy as a minor phase. All phases present are shown in Fig. 3. The data for the annealed $La_{1.9}Mg_{1.1}Ni_9$ alloy are shown as an example and show that it mainly consists of two predominate phases, $(La,Mg)Ni_3$ and $(La,Mg)_2Ni_7$, together with a small residual amount (~2 wt%) of $LaNi_5$ as shown in Fig. 4b.

The abundance of $LaNi_5$ intermetallic decreases appreciably on annealing, while the phase $(La,Mg)_2Ni_4$ completely disappears; instead, the amount of the electrochemically active phases, $(La,Mg)Ni_3$ and $(La,Mg)_2Ni_7$, significantly increases. The phase composition from the SEM microstructural characterization shows a good agreement with the XRD data presented in Tables 1 and 2

A complex multiple phase equilibrium involving a large number of intermetallic constituents present in the La–Mg–Ni-based alloys leads to the multiphase samples when prepared by conventional induction melting. Thus, even during annealing it is difficult to obtain the alloys with a single-phase composition. This is largely because of the diffusion limitations in the migration of atoms in the bulk alloys. Adding Mg can enhance atomic migration in the alloys, thus improving homogeneity, due to the faster kinetics of atomic redistribution and also because the lower melting point of magnesium decreases the temperatures of phase-structural transformations.

As shown in Fig. 4c, the annealed $La_{1.8}Mg_{1.2}Ni_9$ alloy displays a two-phase structure, $(La,Mg)Ni_3$ and $(La,Mg)_2Ni_7$ phases. Furthermore, in comparison with La_2MgNi_9 and $La_{1.9}Mg_{1.1}Ni_9$ alloys, the content of $(La,Mg)Ni_3$ (A region) is relatively much higher than that of $(La,Mg)_2Ni_7$ (B region). This indicates that the increase in Mg/La ratio is a step in the right direction to control the composition of the La–Mg–Ni alloy. In our work [23], we proved that a nearly-homogeneous single $(La,Mg)Ni_3$ phase can be obtained by adding an optimum amount of Mg in the melt and by achieving high cooling rates during the rapid solidification.

The obtained average compositions of $La_{1.9}Mg_{1.1}Ni_9$ and $La_{1.8}Mg_{1.2}Ni_9$ alloys are $La_{1.84}Mg_{1.34}Ni_9$ and $La_{1.83}Mg_{1.48}Ni_9$, which indicates a slight variation in the stoichiometry as compared to the initial stoichiometry (see Figs. S2 and S3 in the Supplementary Information file).

3.2. Hydrogenation characteristics for the annealed alloys

Fig. 5 shows the P–C hydrogen absorption-desorption isotherms for the annealed La_2MgNi_9, $La_{1.9}Mg_{1.1}Ni_9$ and $La_{1.8}Mg_{1.2}Ni_9$ alloys measured at 293 K. As is can be seen, the reversible hydrogen storage capacity of the annealed samples does not show significant differences, being in the range of 1.5–1.6 wt% H. Based on a conversion of the PCT data, the theoretical electrochemical capacity of the annealed alloys corresponds to ~420 mAh g^{-1}.

In the view of practical applications requiring a reversibility of

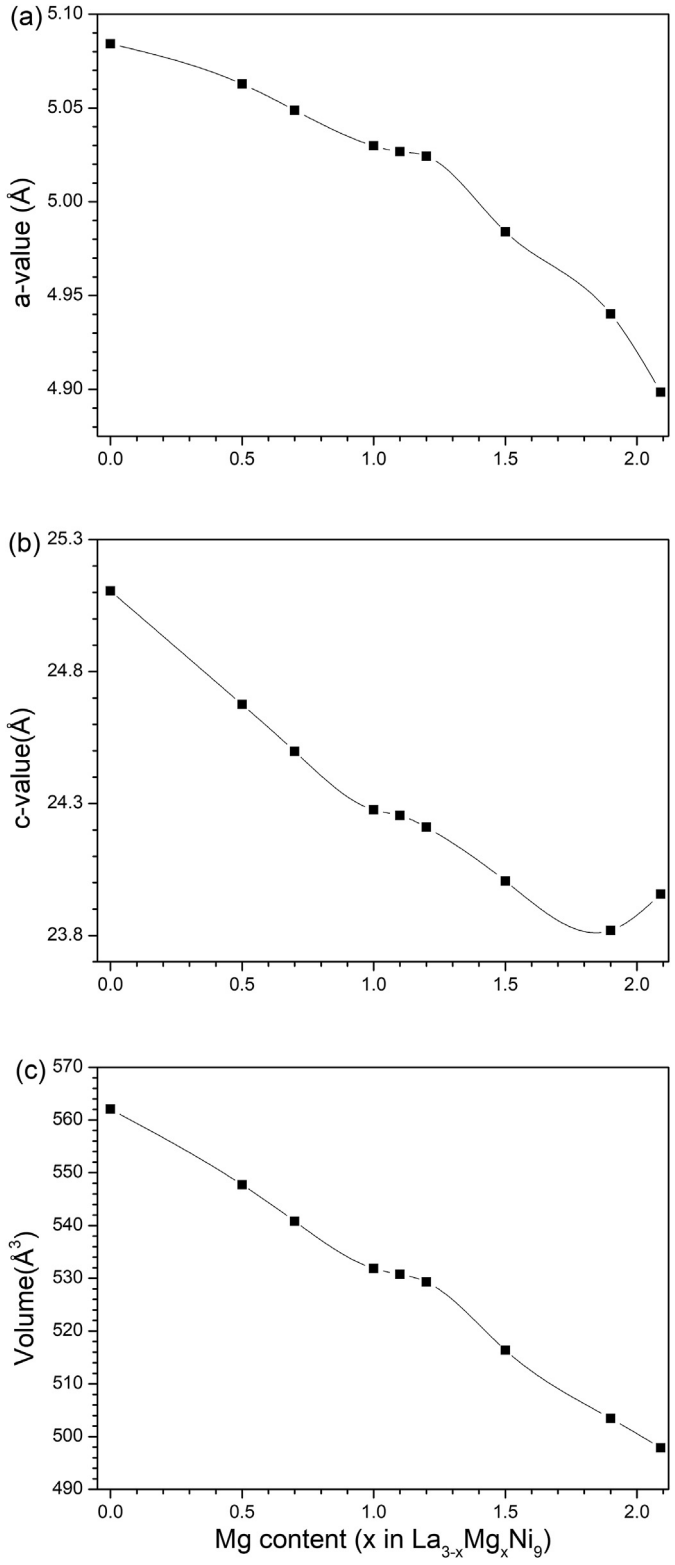

Fig. 2. Metrics of the unit cells of the $La_{3-x}Mg_xNi_9$ (x = 0–2.1) intermetallics as related to the magnesium content.

the H storage performance, among the studied alloys, the annealed La_2MgNi_9 and the $La_{1.9}Mg_{1.1}Ni_9$ alloys have the highest reversible capacity, with a hydrogen desorption capacity of around 1.4 wt% H when measured below 1 bar of equilibrium hydrogen pressure.

The P–C diagrams of hydrogen absorption-desorption for all studied alloys show multi plateau isotherms, which indicate multi-phase compositions in the studied alloys. A comparison of the isotherms shows that increase in Mg content leads to the rise of hydrogen absorption-desorption plateau pressures for the studied alloys. Among the annealed alloys, the $La_{1.8}Mg_{1.2}Ni_9$ alloy has the highest plateau pressure, while the La_2MgNi_9 alloy has the lowest plateau pressure.

According to the earlier reports, the plateau pressures show the following increasing order [31] for the La–Mg–Ni intermetallics: La_2MgNi_9< La_3MgNi_{14}< La_4MgNi_{19}. Thus, for the multicomponent alloys the shape and position of their PCT isotherms will reflect (a) increase of Mg content in the (La,Mg)Ni_2 layer; (b) increase in the content of the $LaNi_5$ layer in the layered structures which is the lowest for La_2MgNi_9, the highest for La_4MgNi_{19} with an intermediate value characteristic for La_3MgNi_{14}.

As expected, for the $La_{1.8}Mg_{1.2}Ni_9$ alloy containing ~89 wt% (La,Mg)Ni_3 with a relatively higher Mg content, the plateau pressure has the highest value, while the La_2MgNi_9 alloy consisting only of the intermetallics with super-stacking structures having a relatively lower Mg content, it has the lowest plateau pressure. Furthermore, presence of $LaNi_5$ in the multiphase alloys is visible in their PCT diagrams which show a shoulder at the highest level of studied pressures. Indeed, the hydrogen plateau pressure of $LaNi_5$ phase is much higher than that for the super-stacking intermetallics [31–34], in appr. 5–10 times. Thus, in spite of rather small amounts, the $LaNi_5$ phase still has a significant influence on the overall plateau pressure shape.

In general, the compositional homogeneity will help to reach a higher value of the reversible hydrogen storage capacity and to achieve a flat shape of plateau pressure isotherm. As the $La_{1.8}Mg_{1.2}Ni_9$ alloy with (La,Mg)Ni_3 as the main composition (~89 wt%), does not exhibit a better performance than the other alloys, this can be related to the fact that at the upper part of the isotherms crosses 1 bar H_2 pressure making the hydride unstable and decreasing the available H discharge capacity. We believe that a higher reversible capacity and lower plateau pressure can be achieved by properly controlling the phase homogeneity and content of Mg in the alloys.

3.3. Electrochemical performance of the annealed alloys

As shown in Fig. 6, the maximum discharge capacities for both annealed La_2MgNi_9 and $La_{1.9}Mg_{1.1}Ni_9$ are close to ~400 mA g^{-1}. In contrast, for the $La_{1.8}Mg_{1.2}Ni_9$ alloy the capacity is very much lower, ~370 mA g^{-1}, at 0.2 C rate (~60 mA/g). The lower discharge capacity of $La_{1.8}Mg_{1.2}Ni_9$ alloy may be ascribed to the lower stability of its hydride, as is evident from the PCT study, see Fig. 5.

The current rate density-dependent electrochemical discharge ability is jointly defined by the maximum electrochemical capacity of the anode material and by the kinetics of electrochemical reactions of hydrogen charge and discharge. This is an important characteristic of the metal hydride anodes as it determines the HRD performance which is one of the most important properties defining practical applications of the MH batteries. The graph presented in Fig. 6d shows the discharge capacities for all studied materials as related to the applied current densities. We note that the La_2MgNi_9 and $La_{1.9}Mg_{1.1}Ni_9$ alloys exhibit higher full discharge capacities (~25% higher) in comparison with the commercial AB_5 alloy (~320 mAh/g; not shown in this paper) measured at the same conditions [22]. In addition, at lower current densities, all the samples display a flatter discharge potential between −0.85 V and −0.9 V vs. the Hg/HgO electrode. This is in a good agreement with the relatively flat plateau pressures observed in the PCT experiments.

As shown in Fig. 6d, with increasing of the discharge current density, the discharge capacities of La_2MgNi_9 and $La_{1.9}Mg_{1.1}Ni_9$

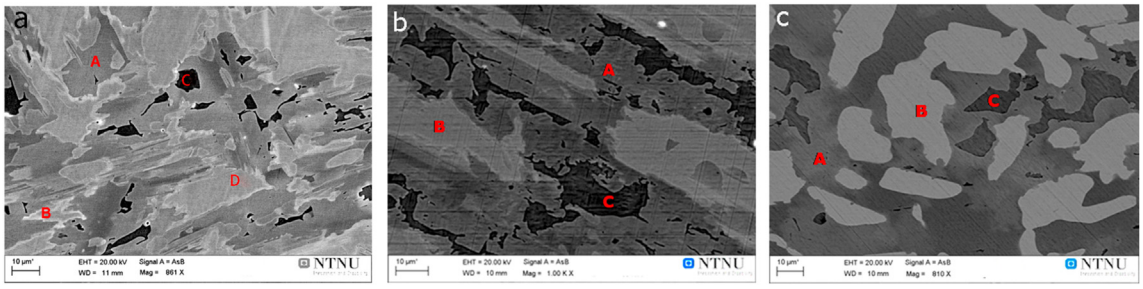

Fig. 3. SEM micrographs of the as-cast La_2MgNi_9 (a) [22], $La_{1.9}Mg_{1.1}Ni_9$ (b) and $La_{1.8}Mg_{1.2}Ni_9$ (c) alloys showing a multi-phase structure containing (La,Mg)Ni_3 (A), $LaNi_5$ (B), $(La,Mg)_2Ni_4$ (C) and $(La,Mg)_2Ni_7$ (D) phases.

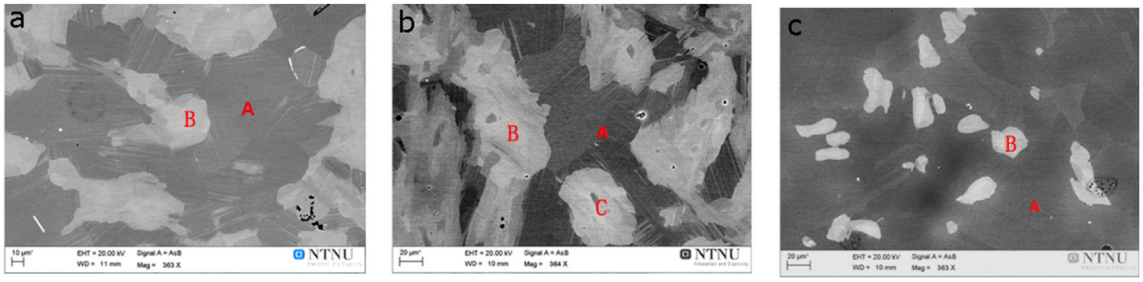

Fig. 4. SEM micrographs of annealed La_2MgNi_9 (a) [22], $La_{1.9}Mg_{1.1}Ni_9$ (b) and $La_{1.8}Mg_{1.2}Ni_9$ (c) alloys at 1223 K for 6 h showing a multi-phase structure containing (La,Mg)Ni_3 (A), $(La,Mg)_2Ni_7$ (B) and $LaNi_5$ (C) phases.

alloys show almost the same variations, while their differences with the $La_{1.8}Mg_{1.2}Ni_9$ alloy become more and more pronounced. With the current density further increasing to 350 mA g^{-1}, the discharge capacities of the annealed La_2MgNi_9, $La_{1.9}Mg_{1.1}Ni_9$ and $La_{1.8}Mg_{1.2}Ni_9$ alloy electrodes decrease to ~340, ~340 and ~300 mAh g^{-1}, respectively. Hence, it can be concluded that the high rate electrochemical discharge capacities of the La_2MgNi_9 and $La_{1.9}Mg_{1.1}Ni_9$ alloys appears to be superior as compared to the $La_{1.8}Mg_{1.2}Ni_9$ alloy.

Fig. 7 shows a comparison of the electrochemical cycling stability of the annealed alloy electrodes during 200 cycles with 100% DOD measured using pasted electrodes. It can be seen that all the alloy electrodes can be fully activated within 3 cycles (see the inset). As shown in Fig. 6 and Table 3, during the cycling at room temperature, the studied pasted electrodes exhibited similar initial discharge capacities C_{in}, La_2MgNi_9 (~345 mAh/g), $La_{1.9}Mg_{1.1}Ni_9$ (~346 mAh/g) and $La_{1.8}Mg_{1.2}Ni_9$ (~340 mAh/g), at 0.33 C (100 mAh/g), which is in agreement with the similarities in their characteristics during storage of gaseous hydrogen.

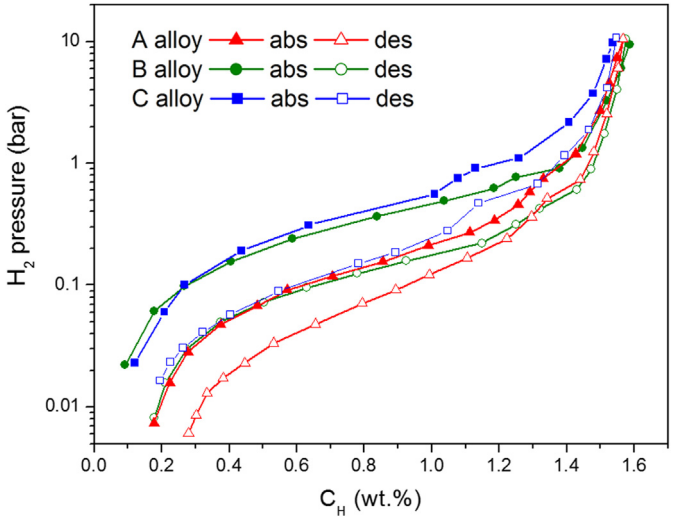

Fig. 5. P–C isotherms of hydrogen absorption-desorption at 293 K for the annealed La_2MgNi_9 (A), $La_{1.9}Mg_{1.1}Ni_9$ (B) and $La_{1.8}Mg_{1.2}Ni_9$ (C) alloys.

Among the studied in the present work electrodes, the annealed La_2MgNi_9 and $La_{1.9}Mg_{1.1}Ni_9$ alloys showed obviously improved cycle life as compared to the annealed $La_{1.8}Mg_{1.2}Ni_9$ alloy during the first 100 cycles. This can be attributed to a higher content of magnesium in the $La_{1.8}Mg_{1.2}Ni_9$ alloy causing its decreased corrosion stability. When the number of the cycles increased to 200, we observe that the cycling stability C_{200}/C_{max} of the $La_{1.9}Mg_{1.1}Ni_9$ alloy electrode is much better than that for the La_2MgNi_9 and $La_{1.8}Mg_{1.2}Ni_9$ alloy electrodes, probably because of a higher amount of the $(La,Mg)_5Ni_{19}$ phase with excellent cycling performance which is present in the multiphase $La_{1.9}Mg_{1.1}Ni_9$ electrode. Liu et al. [13] found that capacity degradation of the single-phase intermetallics decreases following an increase in the $[LaNi_5]/[(La,Mg)_2Ni_4]$ ratio. Thus, the cycling stability improves in the order of $La_2MgNi_9 < La_3MgNi_{14} < La_4MgNi_{19}$.

Faster cycling degradation of the annealed La–Mg–Ni alloys may be related to the oxidation and corrosion of Mg and La, which form Mg and La hydroxides on the fresh particle surfaces during the repeated charge-discharge cycles. The influence of the other factors on oxidation-corrosion of the alloy surfaces and the cycling stability will be studied in our future work focused on probing the effect of using small substitutions of Ni by Co.

As the content of Ni in super layered intermetallics follows the order $La_2MgNi_9 < La_3MgNi_{14} < La_4MgNi_{19}$, changes in the content of Ni with higher electro-catalytic activity can catalyze electrochemical reactions involving structural units in the super-stacking phases [35]. As described above, the increase of Mg content leads to the preferable formation of the (La,Mg)Ni_3 phase and a decrease in the amount of $(La,Mg)_5Ni_{19}$ and $(La,Mg)_2Ni_7$. This contributes to the fact that $La_{1.8}Mg_{1.2}Ni_9$ alloy exhibits relatively inferior properties at high discharge current densities, as compared to other two

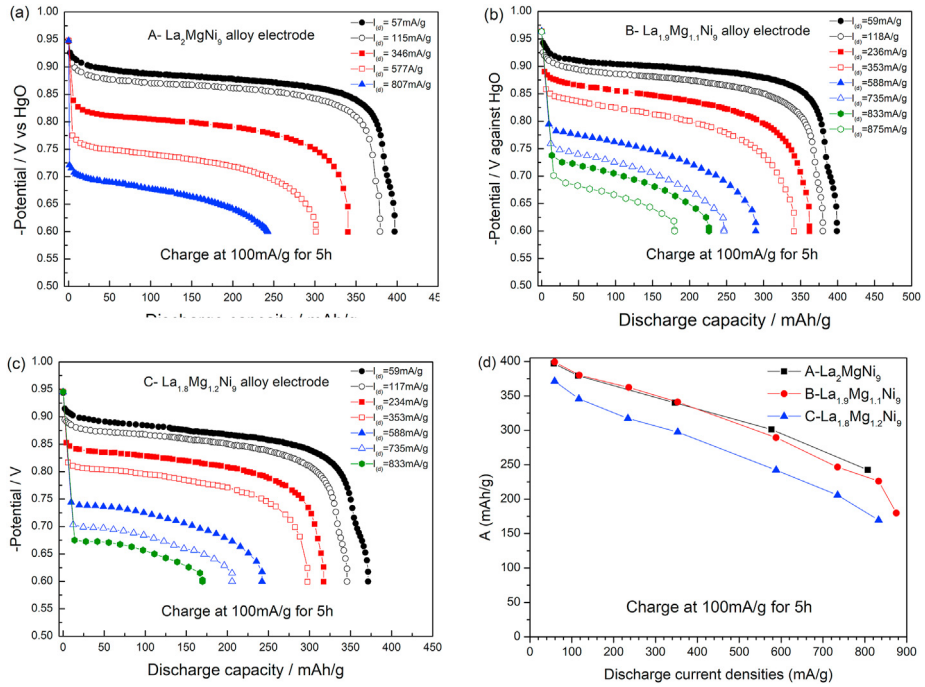

Fig. 6. Discharge curves of the electrodes in the relationship of discharge current densities, for the annealed La_2MgNi_9 (a), $La_{1.9}Mg_{1.1}Ni_9$ (b) and $La_{1.8}Mg_{1.2}Ni_9$ (c) alloys; (d) – Maximum discharge capacity versus applied current density for all three studied alloys.

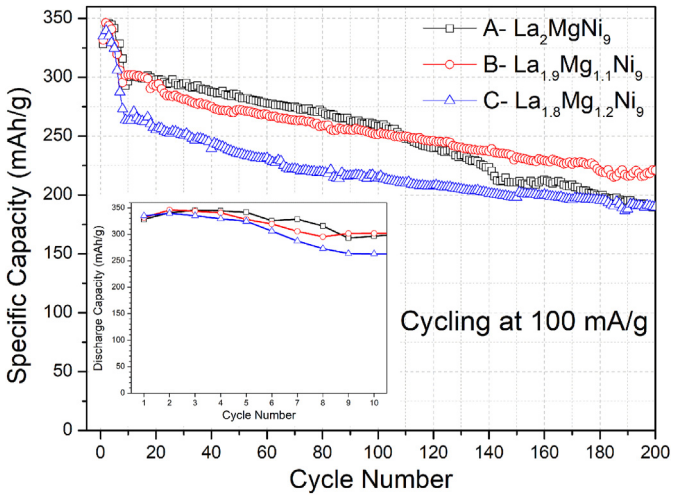

Fig. 7. Comparison of the cycling performance of the pasted electrodes for the annealed La_2MgNi_9, $La_{1.9}Mg_{1.1}Ni_9$ and $La_{1.8}Mg_{1.2}Ni_9$ alloys. The inset shows the first 10 activation cycles. Charging and discharging were performed at 100 mAh/g and room temperature with 100% DOD.

annealed alloys. As shown in Fig. 7b, the $La_{1.9}Mg_{1.1}Ni_9$ alloy shows a high discharge capacity of 175 mAh/g at a high current density of 875 mA/g. This makes the $La_{1.9}Mg_{1.1}Ni_9$ alloy suitable for use at high HRD conditions.

HRD ability of MH/Ni batteries is determined by the kinetics of the hydrogen absorbing/desorbing reactions [36,37]. It is well known that the kinetic performance mainly depends on the charge transfer resistance at the alloy surface and the diffusion rate of the hydrogen atoms in the alloys bulk, which can be estimated by the value of the surface exchange current density (I_0) and diffusion coefficient (D), respectively [38,39]. All the kinetics properties are related to the composition and the microstructure of the hydrogen storage alloys.

The exchange current density (I_0) of the hydride electrode reaction can be calculated according to the linear polarization curves [40], which are described by the following formula [41]:

$$I_0 = \frac{IRT}{F\eta} \quad (1)$$

where R is the gas constant, T is the absolute temperature, I is the applied current density, F is the Faraday constant and η is the overpotential of the electrochemical reaction.

Fig. 8a shows the linear polarization curves of the annealed La_2MgNi_9, $La_{1.9}Mg_{1.1}Ni_9$ and $La_{1.8}Mg_{1.2}Ni_9$ alloy electrodes at 50% DOD and 298 K. When the overpotential is changed within a small range (±10 mV), the current and the overpotential responses show a linear dependence. As listed in Table 3, the exchange current density I_0 increases from 64.2 mA/g (La_2MgNi_9 alloy) to 67.4 mA/g ($La_{1.9}Mg_{1.1}Ni_9$ alloy) and then decreases to 63.3 mA/g ($La_{1.8}Mg_{1.2}Ni_9$ alloy).

Table 3
Summary of the half-cell measurements of the pasted electrodes: Initial capacities before the cycling (C_{in}), Capacity retention after 100 and 200 cycles (C_{100}/C_{max} and C_{200}/C_{in}), Full discharge capacity C_{full} at 0.2 C, HRD ratio at discharge current density of 350 mA/g (HRD_{350}), the exchange current density (I_0), the hydrogen diffusion coefficient (D) and the charge-transfer resistance (R_{ct}).

Annealed alloy	C_{in} mAh/g	C_{100}/C_{max} (%)	C_{200}/C_{max} (%)	C_{full} mAh/g	HRD_{350} (%)	I_0 (mA/g)	D ($\times 10^{-10}$ cm^2/s)	R_{ct} (Ohm)
La_2MgNi_9	345	75.2	55.1	397	85.6	64.2	14.0	1.477
$La_{1.9}Mg_{1.1}Ni_9$	347	72.6	64.1	399	85.3	67.4	16.2	1.525
$La_{1.8}Mg_{1.2}Ni_9$	340	63.2	55.9	371	80.2	63.3	14.2	2.144

Since the $La_{1.9}Mg_{1.1}Ni_9$ alloy shows a superior HRD performance, it can be suggested that the exchange current density I_0 has a direct effect on the HRD performance. This means that the hydrogen oxidation on the surface of alloy electrodes can control the process of HRD performance.

In addition, a lower exchange current density leads to a higher overpotential while the larger overpotential leads to a decrease in useable capacity and an increase in anode corrosion [42]. In other words, the higher exchange current density I_0 of the $La_{1.9}Mg_{1.1}Ni_9$ alloy electrode should result in a higher discharge capacity and a better cycling stability, which well agrees with the electrochemical properties described in Table 3.

The hydrogen diffusion coefficient, which has an important influence on the charging/discharging reactions, was evaluated by using potentiostatic step-size measurements. Fig. 8b shows the semi-logarithmic curves of anodic current vs. time responses of the annealed La_2MgNi_9, $La_{1.9}Mg_{1.1}Ni_9$ and $La_{1.8}Mg_{1.2}Ni_9$ alloy electrodes. In such curves it can be distinguished two regions separated by a black line, as is shown in Fig. 8b. In the first region (0–2000 s), the current dramatically decreases due to the consumption of hydrogen at the surface of the electrode. However, in the second region (>2000 s) the decreasing trend becomes rather gentle and the anodic current (log i) reveals its approximately linear dependence on time (t). The hydrogen diffusion coefficient (D) can be estimated according to the following equation [40,43]:

$$\log i = \log\left(\frac{6FD}{da^2}(C_0 - C_s)\right) - \frac{\pi^2}{2.303}\frac{D}{a^2}t \quad (2)$$

where i, D, C_0, C_s, a, and t are the diffusion current density (A/g), the hydrogen diffusion coefficient (cm^2/s), the initial hydrogen concentration in the bulk of the alloy (mol/cm^3), the hydrogen concentration on the surface of the alloy particles (mol/cm^3), the alloy particle radius (cm), the density of the hydrogen storage alloy (g/cm^3), and the discharge time (s), respectively.

To satisfy the condition for a purely diffusion controlled process, the fully charged electrode was discharged at a constant anodic potential of E = −0.6 V vs. Hg/HgO up to 3600 s. Setting the average particle radius as a = 60 μm, the hydrogen diffusion coefficient D was calculated by using the above equation and tabulated in Table 3. It is found that the hydrogen diffusion coefficient D increases from 20.1×10^{-10} cm^2/s (La_2MgNi_9 alloy) to 23.3×10^{-10} cm^2/s ($La_{1.9}Mg_{1.1}Ni_9$ alloy) and then decreases to 20.5×10^{-10} cm^2/s ($La_{1.8}Mg_{1.2}Ni_9$ alloy). The higher D value of $La_{1.9}Mg_{1.1}Ni_9$ alloy electrode corresponds to its better HRD performance, which indicates that the hydrogen diffusion in the alloy bulk plays a direct role in determining the HRD performance for the annealed La_2MgNi_9, $La_{1.9}Mg_{1.1}Ni_9$ and $La_{1.8}Mg_{1.2}Ni_9$ alloy electrodes.

As mentioned above, the hydrogen diffusion is related to the composition and the microstructure of the hydrogen storage alloys. The $La_{1.9}Mg_{1.1}Ni_9$ alloy electrode with a higher D value contains more phases as compared to the La_2MgNi_9 and $La_{1.8}Mg_{1.2}Ni_9$ alloy electrodes. Because of the higher amount of the available phases and well developed phase boundaries area, this provides more diffusion paths for hydrogen and thus accelerates the hydrogen diffusion [44–46]. In present study the higher exchange current densities (I_0) and hydrogen diffusion coefficient (D) values show their positive impact on the HRD performance of the studied alloy electrodes.

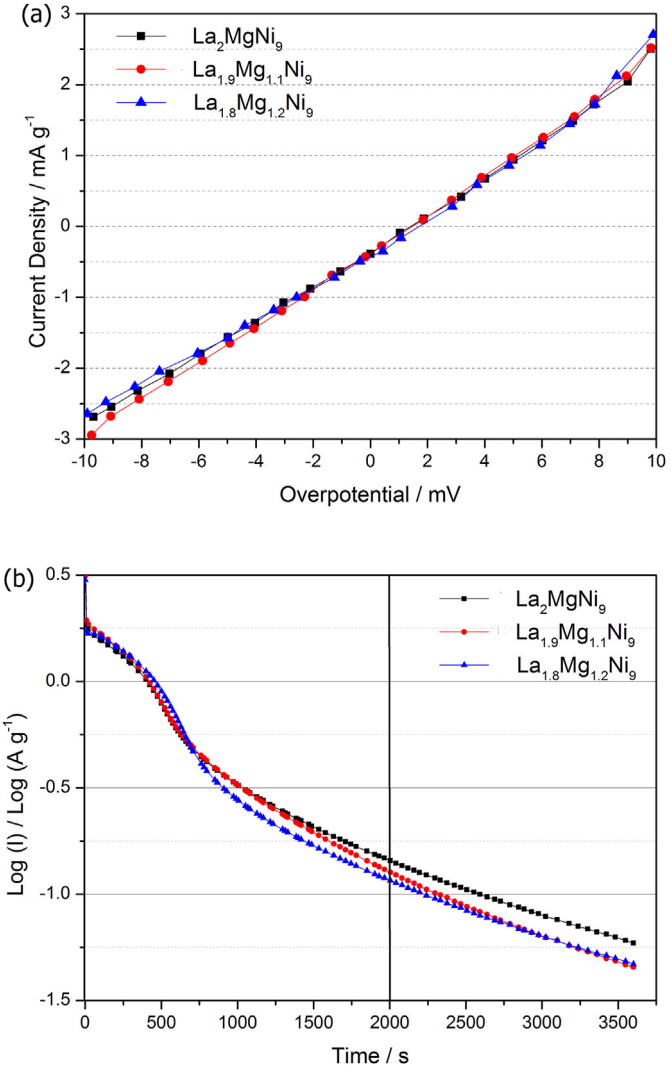

Fig. 8. (a) Linear polarization curves of electrodes measured at 50% DOD and 298 K, (b) Semi-logarithmic plots of anodic current vs. time responses measured at 0.6 V, for the La_2MgNi_9, $La_{1.9}Mg_{1.1}Ni_9$ and $La_{1.8}Mg_{1.2}Ni_9$ alloys alloy electrodes.

4. Conclusions

In the present study, the annealed $La_{3-x}Mg_xNi_9$ (x = 1.0, 1.1 and 1.2) alloys were characterized as H storage and MH battery anode materials to probe the effect of Mg-substitution on the structure, hydrogen absorption-desorption and electrochemical performances of the alloys crystallizing with trigonal $PuNi_3$-type structures.

The following conclusions summarize the results:

The $La_{3-x}Mg_xNi_9$ (x = 1.0, 1.1 and 1.2) alloys were prepared by induction melting and annealed at 1223 K showing a successful formation of $PuNi_3$ type AB_3 layered intermetallics as the major phase constituents. At the highest Mg content a nearly-homogeneous single (La,Mg)Ni_3 phase (~89 wt%) was formed in the $La_{1.8}Mg_{1.2}Ni_9$ alloy.

PCT characterization of the studied alloys showed a gradual destabilisation of the formed hydrides following an increase of the Mg content, with a values of the middle plateaux at 0.085–0.15 bar H_2/293 K.

The maximum discharge capacities of La_2MgNi_9 and $La_{1.9}Mg_{1.1}Ni_9$ alloys are ~400 mA g^{-1} at 0.2 C rate (~60 mA/g) while decreased to ~370 for $La_{1.8}Mg_{1.2}Ni_9$.

The transformations of $(La,Mg)_5Ni_{19}$ 3R/2H → $(La,Mg)_2Ni_7$ → (La,Mg)Ni_3 proceeded during the quenching in all studied alloys. The presence of a higher amount of $(La,Mg)_5Ni_{19}$ and $(La,Mg)_2Ni_7$

phases led to a better cycling stability and an enhanced rate discharge ability.

Superior HRD performances and cycling stability was associated with the synergetic effect of high exchange current density (I_0) and increased values of hydrogen diffusion coefficients (D).

The findings in this work are expected to help in further improvements of the electrochemical properties of La–Mg–Ni alloys based on optimization of their chemical and phase-structural compositions.

CRediT authorship contribution statement

ChuBin Wan: Investigation, Formal analysis, Visualization, Writing - original draft, Writing - review & editing. **Weikang Hu:** Investigation, Formal analysis, Visualization, Writing - original draft. **R.V. Denys:** Investigation, Formal analysis. **C.C. Nwakwuo:** Investigation, Formal analysis. **J.K. Solberg:** Supervision, Formal analysis. **V.A. Yartys:** Conceptualization, Supervision, Writing - review & editing, Project administration, Funding acquisition.

Declaration of competing interest

The authors declare that they have no known competing financial interests or personal relationships that could have appeared to influence the work reported in this paper.

Acknowledgements

This work was supported by the Norwegian Research Council (project 203323 “High Power Batteries Probed by Neutron Scattering”, program SYNKNØYT) and by Institute for Energy Technology (project Q-40704).

The work was also financially supported by the National Natural Science Foundation of China (Grant No. 11975043). ChuBin Wan acknowledges the funding project (No. 201506465019) by China Scholarship Council (CSC).

Appendix A. Supplementary data

Supplementary data to this article can be found online at https://doi.org/10.1016/j.jallcom.2020.157443.

References

[1] M. Hirscher, V.A. Yartys, M. Baricco, J. Bellosta von Colbe, D. Blanchard, R.C. Bowman, D.P. Broom, C.E. Buckley, F. Chang, P. Chen, Y.W. Cho, J.-C. Crivello, F. Cuevas, W.I.F. David, P.E. de Jongh, R.V. Denys, M. Dornheim, M. Felderhoff, Y. Filinchuk, G.E. Froudakis, D.M. Grant, E.M. Gray, B.C. Hauback, T. He, T.D. Humphries, T.R. Jensen, S. Kim, Y. Kojima, M. Latroche, H.-W. Li, M.V. Lototskyy, J.W. Makepeace, K.T. Møller, L. Naheed, P. Ngene, D. Noréus, M.M. Nygård, S.-i. Orimo, M. Paskevicius, L. Pasquini, D.B. Ravnsbæk, M. Veronica Sofianos, T.J. Udovic, T. Vegge, G.S. Walker, C.J. Webb, C. Weidenthaler, C. Zlotea, Materials for hydrogen-based energy storage – past, recent progress and future outlook, J. Alloys Compd. 827 (2020) 153548.

[2] V. Yartys, D. Noreus, M. Latroche, Metal hydrides as negative electrode materials for Ni–MH batteries, Appl. Phys. A 122 (2016) 1–11.

[3] J.-C. Crivello, R.V. Denys, M. Dornheim, M. Felderhoff, D.M. Grant, J. Huot, T.R. Jensen, P. Jongh, M. Latroche, G.S. Walker, C.J. Webb, V.A. Yartys, Mg-based compounds for hydrogen and energy storage, Appl. Phys. A 122 (2016) 1–17.

[4] V.A. Yartys, M.V. Lototskyy, E. Akiba, R. Albert, V.E. Antonov, J.R. Ares, M. Baricco, N. Bourgeois, C.E. Buckley, J.M. Bellosta von Colbe, J.C. Crivello, F. Cuevas, R.V. Denys, M. Dornheim, M. Felderhoff, D.M. Grant, B.C. Hauback, T.D. Humphries, I. Jacob, T.R. Jensen, P.E. de Jongh, J.M. Joubert, M.A. Kuzovnikov, M. Latroche, M. Paskevicius, L. Pasquini, L. Popilevsky, V.M. Skripnyuk, E. Rabkin, M.V. Sofianos, A. Stuart, G. Walker, H. Wang, C.J. Webb, M. Zhu, Magnesium based materials for hydrogen based energy storage: past, present and future, Int. J. Hydrogen Energy 44 (2019) 7809–7859.

[5] J.C. Crivello, B. Dam, R.V. Denys, M. Dornheim, D.M. Grant, J. Huot, T.R. Jensen, P. de Jongh, M. Latroche, C. Milanese, D. Milčius, G.S. Walker, C.J. Webb, C. Zlotea, V.A. Yartys, Review of magnesium hydride-based materials: development and optimisation, Appl. Phys. A 122 (2016) 97.

[6] N.S. Nazer, R.V. Denys, V.A. Yartys, W.-K. Hu, M. Latroche, F. Cuevas, B.C. Hauback, P.F. Henry, L. Arnberg, In operando neutron diffraction study of $LaNdMgNi_9H_{13}$ as a metal hydride battery anode, J. Power Sources 343 (2017) 502–512.

[7] C. Wan, R.V. Denys, V.A. Yartys, In situ neutron powder diffraction study of phase-structural transformations in the La–Mg–Ni battery anode alloy, J. Alloys Compd. 670 (2016) 210–216.

[8] A.A. Volodin, C. Wan, R.V. Denys, G.A. Tsirlina, B.P. Tarasov, M. Fichtner, U. Ulmer, Y. Yu, C.C. Nwakwuo, V.A. Yartys, Phase-structural transformations in a metal hydride battery anode $La_{1.5}Nd_{0.5}MgNi_9$ alloy and its electrochemical performance, Int. J. Hydrogen Energy 41 (2016) 9954–9967.

[9] J. Liu, S. Zhu, H. Cheng, Z. Zheng, Z. Zhu, K. Yan, S. Han, Enhanced cycling stability and high rate dischargeability of A_2B_7-type La–Mg–Ni-based alloys by in-situ formed $(La,Mg)_5Ni_{19}$ superlattice phase, J. Alloys Compd. 777 (2019) 1087–1097.

[10] M. Werwiński, A. Szajek, A. Marczyńska, L. Smardz, M. Nowak, M. Jurczyk, Effect of substitution La by Mg on electrochemical and electronic properties in $La_{2-x}Mg_xNi_7$ alloys: a combined experimental and ab initio studies, J. Alloys Compd. 763 (2018) 951–959.

[11] Y. Zhao, S. Zhang, X. Liu, W. Wang, L. Zhang, Y. Li, S. Han, Phase formation of Ce_5Co_{19}-type super-stacking structure and its effect on electrochemical and hydrogen storage properties of $La_{0.60}M_{0.20}Mg_{0.20}Ni_{3.80}$ (M = La, Pr, Nd, Gd) compounds, Int. J. Hydrogen Energy 43 (2018) 17809–17820.

[12] Y. Zhao, L. Zhang, Y. Ding, J. Cao, Z. Jia, C. Ma, Y. Li, S. Han, Comparative study on the capacity degradation behavior of Pr_5Co_{19}-type single-phase Pr_4MgNi_{19} and La_4MgNi_{19} alloys, J. Alloys Compd. 694 (2017) 1089–1097.

[13] J. Liu, Y. Li, D. Han, S. Yang, X. Chen, L. Zhang, S. Han, Electrochemical performance and capacity degradation mechanism of single-phase La–Mg–Ni-based hydrogen storage alloys, J. Power Sources 300 (2015) 77–86.

[14] R.V. Denys, B. Riabov, V.A. Yartys, R.G. Delaplane, M. Sato, Hydrogen storage properties and structure of $La_{1-x}Mg_x(Ni_{1-y}Mn_y)_3$ intermetallics and their hydrides, J. Alloys Compd. 446–447 (2007) 166–172.

[15] R.V. Denys, A.B. Riabov, V.A. Yartys, M. Sato, R.G. Delaplane, Mg substitution effect on the hydrogenation behaviour, thermodynamic and structural properties of the La_2Ni_7–$H(D)_2$ system, J. Solid State Chem. 181 (2008) 812–821.

[16] R.V. Denys, V.A. Yartys, Effect of magnesium on the crystal structure and thermodynamics of the $La_{3-x}Mg_xNi_9$ hydrides, J. Alloys Compd. 509 (2011) S540–S548.

[17] V. Yartys, R. Denys, Structure–properties relationship in $RE_{3-x}Mg_xNi_9H_{10-13}$ (RE=La,Pr,Nd) hydrides for energy storage, J. Alloys Compd. 645 (2015) S412–S418.

[18] A.A. Volodin, R.V. Denys, G.A. Tsirlina, B.P. Tarasov, M. Fichtner, V.A. Yartys, Hydrogen diffusion in $La_{1.5}Nd_{0.5}MgNi_9$ alloy electrodes of the Ni/MH battery, J. Alloys Compd. 645 (2015) S288–S291.

[19] M. Latroche, F. Cuevas, W.-K. Hu, D. Sheptyakov, R.V. Denys, V.A. Yartys, Mechanistic and kinetic study of the electrochemical charge and discharge of La_2MgNi_9 by in situ powder neutron diffraction, J. Phys. Chem. C 118 (2014) 12162–12169.

[20] Z.J. Gao, B. Zhang, Y.-C. Luo, H.-W. Li, Correlation between phase structure and electrochemical properties of Ce_2Ni_7-type La-RE-Mg-Ni (RE = Nd, Sm, Y) alloys: a comparative study, Journal of the Taiwan Institute of Chemical Engineers 89 (2018) 183–190.

[21] K. Giza, A. Hackemer, H. Drulis, Influence of the synthesis route on hydrogen sorption properties of $La_2MgNi_7Co_2$ alloy, Int. J. Hydrogen Energy 45 (2020) 1492–1498.

[22] W.K. Hu, R.V. Denys, C.C. Nwakwuo, T. Holm, J.P. Maehlen, J.K. Solberg, V.A. Yartys, Annealing effect on phase composition and electrochemical properties of the Co-free La_2MgNi_9 anode for Ni-metal hydride batteries, Electrochim. Acta 96 (2013) 27–33.

[23] C.C. Nwakwuo, T. Holm, R.V. Denys, W. Hu, J.P. Maehlen, J.K. Solberg, V.A. Yartys, Effect of magnesium content and quenching rate on the phase structure and composition of rapidly solidified La_2MgNi_9 metal hydride battery electrode alloy, J. Alloys Compd. 555 (2013) 201–208.

[24] Y. Zhao, X. Liu, S. Zhang, W. Wang, L. Zhang, Y. Li, S. Han, G. Xu, Preparation and kinetic performances of single-phase $PuNi_3$-, Ce_2Ni_7-, Pr_5Co_{19}-type superlattice structure La–Gd–Mg–Ni-based hydrogen storage alloys, Intermetallics 124 (2020) 106852.

[25] C. Wan, V.E. Antonov, R.V. Denys, V.I. Kulakov, V.A. Yartys, $MgCo_2$-D_2 and MgCoNi-D_2 systems synthesized at high pressures and interaction mechanism during the HDDR processing, Prog. Nat. Sci.: Materials International 27 (2017) 74–80.

[26] R.V. Denys, V.A. Yartys, C.J. Webb, Hydrogen in $La_2MgNi_9D_{13}$: the role of magnesium, Inorg. Chem. 51 (2012) 4231–4238.

[27] B.H. Toby, EXPGUI, a graphical user interface for GSAS, J. Appl. Crystallogr. 34 (2001) 210–213.

[28] L. Zhang, J. Wang, W. Du, Y. Ding, Y. Li, S. Yang, S. Han, Y. Fan, The influence of Mg substitution on the phase structure and electrochemical properties of $Nd_{1-x}Mg_xNi_3$ (x = 0.10–0.50) alloys, J. Alloys Compd. 653 (2015) 498–505.

[29] L. Zhang, W. Du, S. Han, Y. Li, S. Yang, Y. Zhao, C. Wu, H. Mu, Study on solid solubility of Mg in $Pr_{3-x}Mg_xNi_9$ and electrochemical properties of $PuNi_3$-type single-phase RE–Mg–Ni (RE=La, Pr, Nd) hydrogen storage alloys, Electrochim. Acta 173 (2015) 200–208.

[30] F.L. Zhang, Y.C. Luo, J.P. Chen, R.X. Yan, J.H. Chen, La–Mg–Ni ternary hydrogen

storage alloys with Ce_2Ni_7-type and Gd_2Co_7-type structure as negative electrodes for Ni/MH batteries, J. Alloys Compd. 430 (2007) 302–307.
[31] J. Matsuda, Y. Nakamura, E. Akiba, Lattice defects introduced into $LaNi_5$-based alloys during hydrogen absorption/desorption cycling, J. Alloys Compd. 509 (2011) 7498–7503.
[32] X.B. Zhang, D.Z. Sun, W.Y. Yin, Y.J. Chai, M.S. Zhao, Crystallographic and electrochemical characteristics of $La_{0.7}Mg_{0.3}Ni_{3-x}(Al_{0.5}Mo_{0.5})_x$ (x=0–0.4) hydrogen storage alloys, Electrochim. Acta 50 (2005) 3407–3413.
[33] M.H. Mendelsohn, D.M. Gruen, A.E. Dwight, $LaNi_{5-x}Al_x$ is a versatile alloy system for metal hydride applications, Nature 269 (1977) 45–47.
[34] A. Draśner, Ž. Blažina, Interaction of hydrogen with the $LaNi_{4.9}In_{0.1}$, $LaNi_{4.8}In_{0.2}$ and $LaNi_{4.8}$ alloys and their Nd analogues, J. Alloys Compd. 420 (2006) 213–217.
[35] Z.Y. Liu, X.L. Yan, N. Wang, Y.J. Chai, D.L. Hou, Cyclic stability and high rate discharge performance of $(La,Mg)_5Ni_{19}$ multiphase alloy, Int. J. Hydrogen Energy 36 (2011) 4370–4374.
[36] M. Tliha, H. Mathlouthi, C. Khaldi, J. Lamloumi, A. Percheron-guegan, Electrochemical properties of the $LaNi_{3.55}Mn_{0.4}Al_{0.3}Co_{0.4}Fe_{0.35}$ hydrogen storage alloy, J. Power Sources 160 (2006) 1391–1394.
[37] F. Feng, D.O. Northwood, Hydrogen diffusion in the anode of Ni/MH secondary batteries, J. Power Sources 136 (2004) 346–350.
[38] M. Raju, M.V. Ananth, L. Vijayaraghavan, Influence of temperature on the electrochemical characteristics of $MmNi_{3.03}Si_{0.85}Co_{0.60}Mn_{0.31}Al_{0.08}$ hydrogen storage alloys, J. Power Sources 180 (2008) 830–835.
[39] D. Barsellini, A. Visintin, W.E. Triaca, M.P. Soriaga, Electrochemical characterization of a hydride-forming metal alloy surface-modified with palladium, J. Power Sources 124 (2003) 309–313.
[40] K. Young, D.F. Wong, T. Ouchi, B. Huang, B. Reichman, Effects of La-addition to the structure, hydrogen storage, and electrochemical properties of C14 metal hydride alloys, Electrochim. Acta 174 (2015) 815–825.
[41] P.H.L. Notten, P. Hokkeling, Double-phase hydride forming compounds: a new class of highly electrocatalytic materials, J. Electrochem. Soc. 138 (1991) 1877–1885.
[42] F. Li, K. Young, T. Ouchi, M.A. Fetcenko, Annealing effects on structural and electrochemical properties of $(LaPrNdZr)_{0.83}Mg_{0.17}(NiCoAlMn)_{3.3}$ alloy, J. Alloys Compd. 471 (2009) 371–377.
[43] G. Zheng, B.N. Popov, R.E. White, Electrochemical determination of the diffusion coefficient of hydrogen through an $LaNi_{4.25}Al_{0.75}$ electrode in alkaline aqueous solution, J. Electrochem. Soc. 142 (1995) 2695–2698.
[44] H. Ye, H. Zhang, W.Q. Wu, T.S. Huang, Influence of the boron additive on the structure, thermodynamics and electrochemical properties of the $MmNi_{3.55-Co_{0.75}Mn_{0.4}Al_{0.3}}$ hydrogen storage alloy, J. Alloys Compd. 312 (2000) 68–76.
[45] R. Tang, L. Liu, Y. Liu, G. Yu, Study on the microstructure and the electrochemical properties of $Ml_{0.7}Mg_{0.2}Ni_{2.8}Co_{0.6}$ hydrogen storage alloy, Int. J. Hydrogen Energy 28 (2003) 815–819.
[46] Y.-H. Zhang, G.-Q. Wang, X.-P. Dong, S.-H. Guo, J.-M. Wu, X.-L. Wang, Investigation on the microstructure and electrochemical performances of $La_2Mg(-Ni_{0.85}Co_{0.15})_9B_x$ (x=0–0.2) hydrogen storage electrode alloys prepared by casting and rapid quenching, J. Alloys Compd. 379 (2004) 298–304.